Check for updates

Hypercrosslinked phenothiazine-based polymers as high redox potential organic cathode materials for lithium–ion batteries†

Ying Zhang,[a] Panpan Gao,[a] Xinya Guo,[a] Han Chen,[a] Ruiqiang Zhang,[a] Ya Du, [iD] *[b] Baofeng Wang [iD] *[a] and Haishen Yang [iD] *[a]

Organic cathode materials have been demonstrated to be highly promising sustainable cathode materials for rechargeable lithium–ion batteries. However, the low redox potentials, low electrical conductivity, and the undesirable dissolution in organic electrolytes greatly limit their applications. Herein, two insoluble hypercrosslinked porous conductive polymers with phenothiazine motifs, **HPEPT** and **HPPT**, were successfully accomplished with high and stable discharge potentials at 3.65 and 3.48 V *versus* Li/Li^{+}. **HPEPT** and **HPPT** with good electrical conductivity exhibited outstanding rate capabilities (up to 800 mA g^{−1}) even at a high mass loading up to 70 wt%. This study shows that excellent organic cathode materials could be achieved readily through this prudent design.

Introduction

Lithium ion batteries (LIBs) with transition-metal-based inorganic cathodes are one of the most popular rechargeable electrochemical energy storage devices (EESDs) and have been extensively used in electric vehicles and smart devices.[1–3] With the increasing demand for EESDs and environmental protection, however, alternatives are highly desirable to substitute the traditional inorganic cathode materials because of their toxicity, resource scarcity, non-sustainability, and limited theoretical capacities.[4–6] Redox-active organic materials, featured with resource abundance, structural diversity, environmental friendliness, tunable properties, and high capacity, *etc.*, are regarded as one of the promising alternative cathode materials for the next-generation EESDs.[7–11] Many efforts have been spent on this research area and made a lot of achievements. Various redox-active functional groups are discovered to date, such as quinones, nitroxyl, phenoxyl, carbazol, hydrazyl, *etc.*[4,10] However, practical applications of organic cathode materials are plagued by many problems, such as the dissolution in organic electrolyte, low electrical conductivity, low redox potential, poor redox cycle stability, *etc.*[12–14] Fortunately, the rich library of redox active motifs and chemical diversification

approaches enable the creation of novel materials with enhanced properties.

Amongst the family of organic redox molecules, phenothiazine is an excellent candidate for organic cathode material due to its brilliant properties. *N*-substituted phenothiazine could reversibly deliver two electrons with average potentials over 4 V *vs.* Li/Li^{+}, and has a theoretical energy density about 1000 W h kg^{−1}, which outperforms commercial inorganic cathodes.[15–18] Furthermore, unlike most of the organic redox-active materials, phenothiazine-based materials demonstrate excellent electrical conductivity, enabling the cathode materials with high redox kinetics.[19–21] Moreover, the cathode materials of phenothiazine-based are p-type electrodes with anions as charge carriers, thus are applicable for various types of metal-ion batteries (*e.g.* Li^{+}, Na^{+}, K^{+}).[15,20] But the p-type cathode materials suffers volume expansion-shrinkage effect during charging-discharging process, caused by the compensation of charges with large anions. This effect might be a serious detriment to the performance of phenothiazine-based rechargeable storage devices.[22] Integration of phenothiazine moieties into a porous polymer with a rigid structure and available pores might be effectively inhibit the adverse effects because of the buffering effect of the pores. Simultaneously, hypercrosslinking of phenothiazine into a rigid porous polymer could dramatically decrease the solubility of the material and thus improve its cycling performances.[17,22] However, the electrical conductivity of porous polymers is known to be extremely low, and usually extra modifications are necessary to warrant their performance as electrode materials.[23,24] But how about a phenothiazine-base porous polymer? Which is a myth to be solved. To the best of our knowledge, to date, there are no reports on phenothiazine-based hypercrosslinked polymers with rigid structure yet.

[a]Shanghai Key Laboratory of Materials Protection and Advanced Materials in Electric Power, College of Environmental and Chemical Engineering, Shanghai University of Electric Power, Shanghai 200090, China. E-mail: yanghsh@shiep.edu.cn; wangbaofeng@shiep.edu.cn

[b]Institute of Advanced Synthesis, School of Chemistry and Molecular Engineering, Nanjing Tech University, Nanjing 211816, China. E-mail: ias_ydu@njtech.edu.cn

† Electronic supplementary information (ESI) available. See DOI: 10.1039/d0ra01312a

With this question in mind, in this work, we synthesized two phenothiazine-functionalized polymeric networks, hyper-crosslinked poly(1,3,5-tris((10-methyl-10H-phenothiazin-3-yl) ethynyl)benzene) (**HPEPT**) and poly(1,3,5-tris(10-methyl-10H-phenothiazin-3-yl)benzene) (**HPPT**) (Scheme 1) and studied their electrochemical properties as cathode materials of LIBs. **HPPT** demonstrated a higher specific surface of 452 m^2 g^{-1} than that of 10 m^2 g^{-1} for **HPEPT** (Fig. S5a and b†). The different linkages in the architecture would affect the topology of the neighboring benzene rings (*e.g.* dihydral angles, active-site distances), and prompt the different conjugation effects and thus instigate the different electric properties, which closely relate to the rate and cycling stability of **HPEPT** and **HPPT**.[25] In comparison with other types of redox-active polymers with analogous structures, **HPEPT** and **HPPT** exhibit much improved electrical conductivity and higher potentials as cathode-active materials in LIBs.[26] The composite electrodes of **HPEPT** and **HPPT** contain a high mass-loading of 70 wt% and present the first stable discharge potentials at 3.65 V and 3.48 V, respectively, and high reversible capacities. For the single electron redox process, the theoretical capacities of **HPEPT** and **HPPT** are 87 and 103 mA h g^{-1}, respectively, and the theoretical energy densities of **HPEPT** and **HPPT** are 330 and 367 W h kg^{-1}, respectively, which are among the highest in the organics. The theoretical energy densities are more than double for two electron redox processes.[17]

Experimental

Material synthesis

As shown in Scheme 2, **HPEPT** and **HPPT** are synthesized from the same intermediate **1**, which was prepared in four steps from commercially available phenothiazine. The synthetic details of **1** can be found in ESI.†[27–31] **HPEPT** and **HPPT** were synthesized by using Sonogashira coupling reaction and acetylene trimerization reaction, respectively, as follow.[32,33]

HPEPT.[32] Prepared compound **1** (0.40 g, 1.53 mmol), 1,3,5-tribromobenzene (0.32 mg, 1.02 mmol), Pd(PPh$_3$)$_2$Cl$_2$ (35.80 mg, 0.05 mmol) and CuI (9.71 mg, 0.05 mmol) were dissolved in Et$_3$N (6 mL) and anhydrous THF (20 mL) in a 100 mL Schlenk flask. The solution was refluxed at 120 °C for 12 h under nitrogen atmosphere. After cooling, the precipitate was collected by filtration and washed with water (100 mL), methanol (100 mL), ethanol (100 mL), ether (100 mL) and acetone (100 mL). The brown powder obtained was Soxhlet extracted with dichloromethane for 24 h and dried at 120 °C under *vacuo* conditions overnight, afforded **HPEPT** (0.47 g, yield: 99%) as a brown powder. FT-IR ν_{max}/cm^{-1} 1601 (CC), 1574
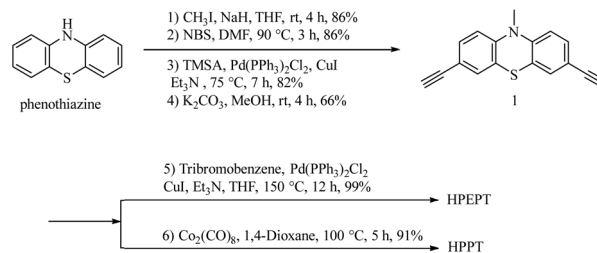
Scheme 2 Synthesis of **HPEPT** and **HPPT**.

(CC), 1467 (CH), 1260 (CN), 879 (CH) 810 (CH); elemental analysis (%) for (C$_{51}$H$_{33}$N$_3$S$_3$)$_n$: C, 78.13; N, 5.36; H, 4.24; S, 12.27. Found: C, 62.87; N, 3.93; H, 3.12; S, 14.99. The elemental analysis results obtained are different from the expected values, which may be due to incomplete combustion of the carbon-rich network structure.[32]

HPPT.[33] Prepared compound **1** (1.00 g, 3.83 mmol) and Co$_2$(CO)$_8$ (0.33 g, 0.96 mmol) were dissolved in anhydrous 1,4-dioxane (40 mL) in a 100 mL Schlenk flask. The solution was refluxed at 100 °C for 5 h under nitrogen atmosphere. After cooling, the precipitate was collected by filtration and washed with water (100 mL), methanol (100 mL), ethanol (100 mL), ether (100 mL) and acetone (100 mL). The brown powder obtained was Soxhlet extracted with dichloromethane for 24 h and dried at 120 °C under *vacuo* conditions overnight, afforded **HPPT** as a brown powder (0.91 g, yield: 91%). FT-IR ν_{max}/cm^{-1} 1602 (CC), 1580 (CC), 1459 (CH), 1258 (CN), 878 (CH), 808 (CH); elemental analysis (%) for (C$_{45}$H$_{33}$N$_3$S$_3$)$_n$: C, 75.92; N, 5.90; H, 4.67; S, 13.51. Found: C, 67.66; N, 4.78; H, 2.81; S, 10.22. The elemental analysis results obtained are different from the expected values, which may be due to incomplete combustion of the carbon-rich network structure.[32]

Electrochemical measurements

The electrochemical tests of **HPEPT** and **HPPT** as cathode active materials were assembled in an argon-filled glove box using 2016 coin-type cells. The composite electrodes containing 70 wt% as-prepared polymers, 20 wt% acetylene black, 10 wt% PVDF binder in N-methyl-2-pyrrolidone (NMP). The obtained mixture was coated on aluminum foil and dried at 80 °C for 12 h. The dried electrode was cut into a round shape of 14 mm in diameter and the as-prepared polymers mass loading is about 1 mg cm^{-2}. The cells were assembled with lithium metal as the anode electrode, polypropylene film (Celgard 2400) as the separator, and 1 M LiPF$_6$ in EC/DMC/EMC (1 : 1 : 1 by volume) as the electrolyte. Electrochemical cyclic voltammetry (CV) and electrochemical impedance spectroscopy (EIS) tests were performed at an electrochemical workstation (CHI660E). The charge–discharge cycles were carried out on a Neware Battery Test System.

Results and discussion

The obtained **HPEPT** and **HPPT** were characterized by FT-IR, elemental analysis, TGA, SEM and PXRD analysis. The FT-IR
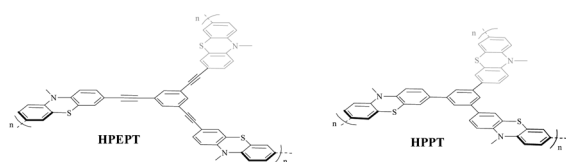
Scheme 1 Structures of HPEPT and HPPT.

spectra of **HPEPT** and **HPPT** are similar (Fig. 1a). The absorption bands at 3277, 657 and 594 cm^{-1} in FT-IR spectra of **1** are assigned to the C–H stretching and bending vibration of the terminal alkynes, while the signal at 2109 cm^{-1} with low intensity is assigned to the C≡C stretching vibration (Fig. 1a). The disappearance of the above peaks in FT-IR spectra of **HPEPT** and **HPPT** indicates the successful polymerization of monomer **1**. The bands at 1603–1459 cm^{-1} are the C=C stretching vibration in benzene ring. The bands at 1340–1043 cm^{-1} are the stretching vibration of the C–N and C–S. The bands in the fingerprint region around 883–805 cm^{-1} are assigned to the C–H bending vibration from 1,2,4-trisubstituted in benzene ring. The infrared spectra of **HPEPT** shows the bands at 1601 and 1574 cm^{-1}, attributing to the C=C stretching vibrations of the benzene ring. While the corresponding bands for **HPPT** are slightly blue shift to 1602 and 1580 cm^{-1}, suggesting different conjugation effects of **HPEPT** and **HPPT**.

The morphology of **HPEPT** and **HPPT** confirmed by scanning electron microscopy (SEM) images, indicating the relatively uniform micron-sized spheres (Fig. 1b and c). The thermal stabilities of **HPEPT** and **HPPT** were tested by using thermal gravimetric analysis (TGA) (Fig. S6a and b†). In Fig. S6a,† samples were heated from room temperature to 800 °C at a heating rate of 10 °C min^{-1} under nitrogen atmosphere. **HPEPT** and **HPPT** are thermally stable up to 372 °C and 421 °C, respectively (indicated by the 20% weight loss). TGAs tested in air indicated that the materials could be oxidized at about 200 °C and begin to decompose at about 400 °C (Fig. S6b†). The high thermal stability is crucial to the safety of rechargeable batteries. XRD patterns of **HPEPT** and **HPPT** establish the amorphous characters of **HPEPT** and **HPPT** (Fig. S7†).

As shown in Scheme 3, the redox activity of **HPEPT** and **HPPT** can be represented as *N*-substituted phenothiazine, whose redox mechanism involves a two successive one-electron oxidation process.[15,34,35] The first stage oxidation of a neutral state leads to the formation of a radical cation (oxidized stage I), the second stage oxidation leads to the formation of oxidized stage II. These charges are compensated by electrolyte anions (PF$_6$$^-$).[18]

The two-step reaction is also confirmed from the cyclic voltammetry (CV) measurement of **HPEPT** and **HPPT**. As shown in
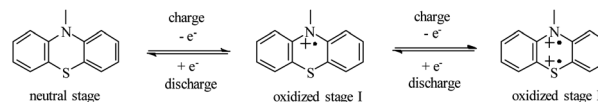
Scheme 3 The electrochemical redox mechanism of the phenothiazine derivatives.

Fig. 2a and b (dashed line), **HPEPT** and **HPPT** exhibited the redox process of two electrons in the potential range of 3–4.7 V at the scan rate of 1 mV s^{-1} in the first cycle. As shown in Fig. 2a, **HPEPT** exhibited two oxidation peaks at 3.93 V and 4.54 V in the oxidation process and only one distinct reduction peak at 3.51 V in the reduction process. While **HPPT** have two oxidation peaks at 3.74 V and 4.37 V in the oxidation process, and together with two distinct reduction peaks at 3.52 V and 4.16 V in the reduction process (Fig. 2b). As can be seen from Fig. 2a and b, the redox processes of **HPEPT** and **HPPT** in this broad potential range are not completely reversible, possibly caused by the insufficient stability of electrolytes at high potential.[17] Thereby, the electrochemical performances of **HPEPT** and **HPPT** were further investigated between 3 and 4.2 V/Li/Li$^+$.

The CV studies of **HPEPT** and **HPPT** in the potential range 3–4.2 V at the scan rate of 1 mV s^{-1} are shown in Fig. 2a and b (full line). As shown in Fig. 2a, in the initial state, **HPEPT** has an anodic peak at 3.92 V and a cathodic peak at 3.52 V. The potential separation between the peaks is about 0.40 V. While **HPPT** has a slightly lower anodic peak at 3.78 V and a closely cathodic peak at 3.47 V (Fig. 2b). The narrower peak potential separation (about 0.31 V) indicates that **HPPT** has a lower electrode polarization than that of **HPEPT** during the
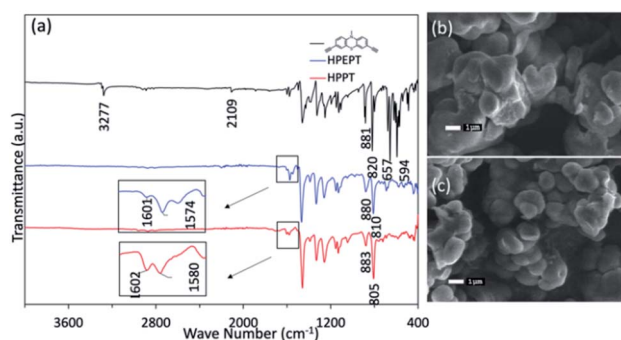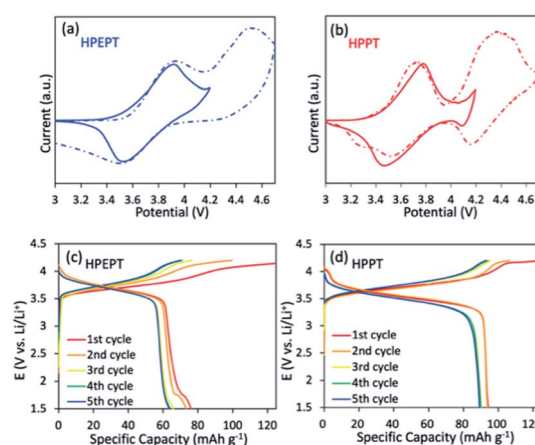
Fig. 2 (a) Cyclic voltammograms of **HPEPT** in cell involves the first redox process (blue full line) in the voltage range of 3–4.2 V *vs.* Li/Li$^+$ and the two redox process (blue dashed line) in the voltage range of 3–4.7 V *vs.* Li/Li$^+$ at 1 mV s^{-1}. (b) Cyclic voltammograms of **HPPT** in cell involves the first redox process (red full line) in the voltage range of 3–4.2 V *vs.* Li/Li$^+$ and the two redox process (red dashed line) in the voltage range of 3–4.7 V *vs.* Li/Li$^+$ at the scan rate of 1 mV s^{-1}. (c) Discharge–charge curves of **HPEPT** with pre-activated 1st and 2nd cycles at 100 mA g^{-1} and 3rd, 4th, 5th cycles at 200 mA g^{-1}. (d) Discharge–charge curves of **HPPT** with pre-activated 1st and 2nd cycles at 100 mA g^{-1} and 3rd, 4th, 5th cycles at 200 mA g^{-1}.

Fig. 1 (a) FT-IR spectra of **1**, **HPPT** and **HPEPT**. (b) SEM image of **HPEPT**. (c) SEM image of **HPPT**.

electrochemical process under the same condition. This observation can be explained by the higher porous nature of **HPPT**, which allows the easier transportation of electrolyte ions and improves the electrochemical kinetics. The anodic and cathodic peaks of **HPEPT** and **HPPT** of the first three cycles are similar, indicating the robust stability and reversibility electrochemical performance of **HPEPT** and **HPPT** (see in Fig. S8†). While the potential separation between the redox peaks of each cycle becomes narrower with the progressing, indicating the activation processes in the beginning. The higher oxidation and reduction peaks of **HPEPT** than those of **HPPT** are possibly due to the relative electron-deficient C≡C groups in **HPEPT**. C≡C bond is sp-hybridized electron-withdrawing group that helps to increase the working voltage of the material.

The galvanostatic charge–discharge curves of **HPEPT** and **HPPT** in coin-type cells were measured at a current density of 200 mA g^{-1} and a potential window of 1.5–4.2 V with pre-activated 2 cycles at 100 mA g^{-1} (Fig. 2c–d). As shown in Fig. 2c, **HPEPT** displays an average discharge voltage plateau at about 3.65 V and a charge voltage plateau at about 3.81 V after 5 cycles. In comparison, the **HPPT** exhibits a relatively lower but longer discharge voltage plateau at about 3.48 V and a charge voltage plateau at about 3.76 V under the same conditions (Fig. 2d). The experimental results correspond with the CV curves.

The cycling behavior of **HPEPT** and **HPPT** at 200 mA g^{-1} is shown in Fig. 3a. Initial discharge capacity of **HPPT** is 90 mA h g^{-1} (87% of the theoretical capacity). While **HPEPT** shows relatively lower initial capacity of 66 mA h g^{-1} (76% of the theoretical capacity). The discharge capacities of **HPPT** could reach 76 mA h g^{-1} after 200 cycles and capacity retention of **HPPT** is 85%, which are much higher than those of **HPEPT** (43 mA h g^{-1} and 66%, respectively). The coulombic efficiency for **HPPT** reaches above 95% after 4 cycles, which is better than that of **HPEPT** (after 15 cycles reaches above 95%). The excellent cycling stabilities of **HPEPT** and **HPPT** could be attributed to the rigid robust structures of **HPEPT** and **HPPT** and their efficient

inhibition of the volume expansion-shrinkage effect during charging–discharging processes. Furthermore, the hyper-crosslinked polymers are insoluble in the organic electrolytes, which are also beneficial to the cycling capabilities. The relatively superior cycling stability of **HPPT** than that of **HPEPT** could be explained by its more efficient crosslinked architecture, indicative by its higher specific surface area and more available channels in **HPPT**, which also accounts for their different percentages of active-site utilization.

The rate performance of **HPEPT** and **HPPT** was tested at a current density of 200, 400 and 800 mA g^{-1}. As compared to most other types of redox-active polymers with analogous structures, as shown in Fig. 3b and c, both polymers exhibited excellent rate performances even at high current density up to 800 mA g^{-1}, ascribed to the conductive properties of the Fig. 3b and c show the capacity of **HPEPT** and **HPPT** decreases as current density increases. The specific capacity of **HPEPT** was 52, 40, 29 mA h g^{-1} at 200, 400, and 800 mA g^{-1} after 10 cycles, whereas **HPPT** presents superior reversible capacities of 93, 87, and 75 mA h g^{-1} at 200, 400, and 800 mA g^{-1}. The specific capacity of **HPPT** material still reached 91 mA h g^{-1} when returned to 200 mA g^{-1} with 98% capacity retention. This result demonstrates that **HPPT** electrodes possess high rate capability than that of **HEPPT**. Again, this result could be attributed to the relative higher porosity and open transportation channels of **HPPT**.

Conclusions

In summary, we successfully synthesized two novel insoluble rigid hypercrosslinked phenothiazine-functionalized polymers (**HPEPT** and **HPPT**) and studied their applications as organic cathode materials of lithium ion batteries. These phenothiazine-based p-type polymers, **HPEPT** and **HPPT**, inherit the excellent electrochemical properties from their parent monomers, and possess reversible redox activity with high discharge potentials at 3.65 and 3.48 V, respectively. More importantly, the porous **HPPT** obtained with pretty high specific surface area (S_{BET}: 452 m^2 g^{-1}) still maintains high electric conductivity as the linear phenothiazine-based polymers have, enabling the material with high redox kinetics and efficient active-site utilization (87% of the theoretical capacity) without any further modification. Moreover, the porous hyper-crosslinked polymers with rigid structure could effectively inhibit volume expansion-shrinkage effect of the p-type electrode materials, and endow the improved cycling stability. The discovery herein opens a new direction for development of novel organic electrode materials.

Conflicts of interest
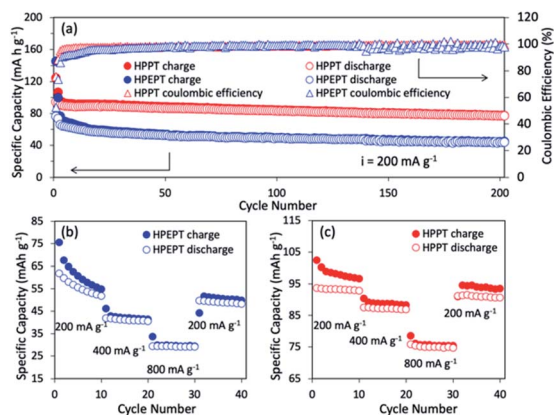
There are no conflicts to declare.

Acknowledgements

Fig. 3 (a) Cycling performance of HPEPT and HPPT at a current density of 200 mA g^{-1}. The cell was pre-activated 2 cycles at 100 mA g^{-1} before starting the measurements. (b) Rate capability of HPEPT. (c) Rate capability of HPPT.

Notes and references

1 M. Armand and J.-M. Tarascon, *Nature*, 2008, **451**, 652–657.
2 P. L. Taberna, S. Mitra, P. Poizot, P. Simon and J. M. Tarascon, *Nat. Mater.*, 2006, **5**, 567–573.
3 V. Etacheri, R. Marom, R. Elazari, G. Salitra and D. Aurbach, *Energy Environ. Sci.*, 2011, **4**, 3243–3262.
4 S. Muench, A. Wild, C. Friebe, B. Haupler, T. Janoschka and U. S. Schubert, *Chem. Rev.*, 2016, **116**, 9438–9484.
5 M. S. Whittingham, *Chem. Rev.*, 2004, **104**, 4271–4301.
6 S. Zhang, W. Huang, P. Hu, C. Huang, C. Shang, C. Zhang, R. Yang and G. Cui, *J. Mater. Chem. A*, 2015, **3**, 1896–1901.
7 B. Dunn, H. Kamath and J.-M. Tarascon, *Science*, 2011, **334**, 928–935.
8 Y. Zhao, Y. Ding, Y. Li, L. Peng, H. R. Byon, J. B. Goodenough and G. Yu, *Chem. Soc. Rev.*, 2015, **44**, 7968–7996.
9 J. Winsberg, T. Hagemann, T. Janoschka, M. D. Hager and U. S. Schubert, *Angew. Chem., Int. Ed.*, 2017, **56**, 686–711.
10 R. Gracia and D. Mecerreyes, *Polym. Chem.*, 2013, **4**, 2206–2214.
11 Q. He, C. Zhang, X. Li, X. Wang, P. Mu and J. Jiang, *Acta Chim. Sin.*, 2018, **76**, 202–208.
12 K. Pirnat, J. Bitenc, A. Vizintin, A. Krajnc and E. Tchernychova, *Chem. Mater.*, 2018, **30**, 5726–5732.
13 X. Liu and A. Du, *Chin. Polym. Bull.*, 2017, **8**, 78–85.
14 Y. Zhang, J. Wang and S. N. Riduan, *J. Mater. Chem. A*, 2016, **4**, 14902–14914.
15 M. Kolek, F. Otteny, P. Schmidt, C. Mück-Lichtenfeld, C. Einholz, J. Becking, E. Schleicher, M. Winter, P. Bieker and B. Esserb, *Energy Environ. Sci.*, 2017, **10**, 2334–2341.
16 C. Zhang, Z. Niu, S. Peng, Y. Ding, L. Zhang, X. Guo, Y. Zhao and G. Yu, *Adv. Mater.*, 2019, **31**, 1901052.
17 T. Godet-Bar, J. C. Lepretre, O. Le Bacq, J. Y. Sanchez, A. Deronzier and A. Pasturel, *Phys. Chem. Chem. Phys.*, 2015, **17**, 25283–25296.
18 R. Guilmin, F. Alloin, F. Molton and J.-C. Leprêtre, *Electrochim. Acta*, 2017, **232**, 182–191.
19 S. Ergun, C. F. Elliott, A. P. Kaur, S. R. Parkin and S. A. Odom, *Chem. Commun.*, 2014, **50**, 5339–5341.
20 M. Lee, J. Hong, B. Lee, K. Ku, S. Lee, C. B. Park and K. Kang, *Green Chem.*, 2017, **19**, 2980–2985.
21 T. Shimizu, K. Yamamoto, P. Pandit, H. Yoshikawa and S. Higashibayashi, *Sci. Rep.*, 2018, **8**, 579.
22 F. Otteny, M. Kolek, J. Becking, M. Winter, P. Bieker and B. Esser, *Adv. Energy Mater.*, 2018, **8**, 1802151.
23 Y. Zhang, S. N. Riduan and J. Wang, *Chem.–Eur. J.*, 2017, **23**, 16419–16431.
24 Y. Zhong, Y. Yang, Y. Shen, W. Xu, Q. Wang, A. L. Connor, X. Zhou, L. He, X. C. Zeng, Z. Shao, Z. L. Lu and B. Gong, *J. Am. Chem. Soc.*, 2017, **139**, 15950–15957.
25 C. Su, H. He, L. Xu, K. Zhao, C. Zheng and C. Zhang, *J. Mater. Chem. A*, 2017, **5**, 2701–2709.
26 J. Xie, W. Chen, G. Long, W. Gao, Z. J. Xu, M. Liu and Q. Zhang, *J. Mater. Chem. A*, 2018, **6**, 12985–12991.
27 R. Krishna, V. Kurshev and L. Kevan, *Phys. Chem. Chem. Phys.*, 1999, **1**, 2833–2839.
28 R. M. Pearson, C. H. Lim, B. G. McCarthy, C. B. Musgrave and G. M. Miyake, *J. Am. Chem. Soc.*, 2016, **138**, 11399–11407.
29 A. Arnanz, C. Moreno, M.-L. Marcos, J. González-Velasco and S. Delgado, *Eur. J. Inorg. Chem.*, 2007, **2007**, 5215–5225.
30 Q. Chen, Y. Ma, C. Wang and Y. Shen, *Chin. J. Org. Chem.*, 2012, **32**, 1526–1532.
31 P. K. Mandali and D. K. Chand, *Catal. Commun.*, 2014, **47**, 40–44.
32 Y. Zhu, H. Yang, Y. Jin and W. Zhang, *Chem. Mater.*, 2013, **25**, 3718–3723.
33 M. H. Weston, O. K. Farha, B. G. Hauser, J. T. Hupp and S. T. Nguyen, *Chem. Mater.*, 2012, **24**, 1292–1296.
34 A. Golriz, T. Suga, H. Nishide and R. B. a. J. Gutmann, *RSC Adv.*, 2015, **5**, 22947–22950.
35 P. Acker, L. Rzesny, C. F. N. Marchiori, C. M. Araujo and B. Esser, *Adv. Funct. Mater.*, 2019, **29**, 1906436.